

Advance Publication by J-STAGE
Journal of Reproduction and Development

Accepted for publication: April 15, 2020

Advanced Epub: April 28, 2020

1 **Repeated hyperstimulation affects the ultrastructure of**
2 **mouse fallopian tube epithelium**

3

4 Sevastiani Antonouli^{1, *}, Maria Grazia Palmerini^{1, *}, Serena Bianchi¹, Gianna Rossi¹, Sandra
5 Cecconi¹, Manuel Belli¹, Sara Bernardi¹, Mohammad Ali Khalili², Giuseppe Familiari³,
6 Stefania Annarita Nottola³, Guido Macchiarelli¹

7

8 ** These authors contributed equally*

9 ¹Dept. of Life, Health and Environmental Sciences. University of L'Aquila, L'Aquila, Italy;

10 ²Dept. of Reproductive Biology, Yazd Institute for Reproductive Sciences. Shahid Sadoughi
11 University of Medical Sciences, Yazd, Iran.

12 ³Dept. of Anatomy, Histology, Forensic Medicine and Orthopaedics. University of Rome La
13 Sapienza, Rome, Italy;

14

15 *Corresponding author:*

16 *Prof. Maria Grazia Palmerini*, Dept. of Life, Health and Environmental Sciences. University
17 of L'Aquila, Via Vetoio, 67100, L'Aquila, Italy.

18 e-mail: mariagrazia.palmerini@univaq.it

19

20 **Short title:** Morphology of hyperstimulated ampullae

21

22 **ABSTRACT**

23 Controlled ovarian hyperstimulation (COH) is routinely used in assisted reproductive
24 technologies (ARTs) to increase the yields of mature oocytes. The possibility that patients
25 with a history of failures or poor-responders may develop side-effects following these
26 treatments is still debated. Epidemiological studies reported controversial results about
27 pregnancy outcome and the risk of developing gynecological cancers. By using a mouse
28 model, here we compared the ultrastructural features of Fallopian tubes (FTs) obtained from
29 mice undergoing or not (control, CTR) four (4R) and eight (8R) rounds of gonadotropin
30 stimulation.

31 Although the morphological characteristics of oviductal layers seemed unaffected by
32 repeated treatments, dose-response ultrastructural alterations in the ampulla appeared in the
33 4R group and even more in the 8R group. The targets were oviductal ciliated (CCs) and non-
34 ciliated (NCCs) cells, which showed damaged mitochondria and glycogen accumulations in
35 the cytoplasm. The drastic reduction of CCs, evident after 4R, was supported by the absence
36 of cilia. After 8R, glycogen granules were significantly reduced and massive degeneration of
37 mitochondria, which appeared swollen and/or vacuolated, occurred in NCCs. Moreover,
38 disintegrated mitochondria were found at the periphery of mitophagic vacuoles with evident
39 signs of cristolysis. The morphometric analysis evidenced a significant increase in the density
40 and frequency of damaged mitochondria after 4R and 8R. The absence of cilia, necessary to
41 sustain oviductal transport of oocytes, spermatozoa and embryos, may originate from either
42 mitochondrial dysfunction or glycogen consumption.

43 These results suggest that repeated COH treatments could induce alterations impairing
44 fertilization and embryo transport toward the uterus.

45 **Keywords:** mouse, fallopian tubes, controlled ovarian hyperstimulation, columnar epithelial
46 cells, electron microscopy.

47

48 **INTRODUCTION**

49 Controlled ovarian hyperstimulation (COH) is routinely used in Assisted
50 Reproductive Technologies (ARTs) to increase the number of retrieved mature oocytes and,
51 therefore, to enhance the success rate of these protocols [1]. However, increased number of
52 treatments ($n>4$), especially with gonadotropins, can induce complications in treated patients,
53 including premature progesterone elevation throughout the follicular phase, defective
54 endometrium receptivity, luteal phase insufficiency or severe ovarian hyperstimulation
55 syndrome (OHSS) [2-4]. Although the relationship between hyperstimulation and cancer is
56 still controversial [5-6], a major risk is that COH-induced supraphysiologic estrogen (E2)
57 levels may promote, with time, the growth of estrogen-sensitive tumors, such as endometrial,
58 ovarian and estrogen receptor-positive breast cancers [7-9].

59 An interesting question is how fallopian tubes (FTs) could respond to COH. Indeed, during
60 the reproductive cycle, hormonal oscillations impact on the histophysiology of the FTs and,
61 specifically, of the *tunica mucosa* [10, 11]. In mice, the relationship between the number of
62 columnar epithelial ciliated cells and non-ciliated cells - also known as secretory, intercalar
63 or peg cells - changes during the hormonal cycle with the predominance of ciliated cells
64 during the follicular phase and of secretory cells during the luteal phase, even if with
65 individual differences [12]. In this species, E2 stimulates epithelial cell hypertrophy, cilia
66 beat frequency (CBF) and oviductal secretions [13], while progesterone (P) acts on *tunica*
67 *mucosa* by inducing epithelial cell atrophy, deciliation and decrease of CBF [14, 15]. If P
68 production is altered, a delay in the transportation timing of the ovum or zygotes occurs [16].
69 In our previous papers, we analyzed oocyte spindle morphology and the content of proteins
70 involved in cell cycle control in ovaries and FTs retrieved from mice treated up to 8 times (8

71 Rounds, 8R) with a standardized protocol of gonadotropin [17, 18]. Despite after 4R the only
72 modification recorded was an increase in cyclin D1 content in FT, after 8R also p53,
73 phospho-p53, phospho-AKT, GSK3B and OCT3/4 contents were significantly higher than
74 in controls. The over-expression of these proteins, all involved in the control of cell cycle
75 progression, and the drastic decrease of oocyte number and spindle quality strongly
76 supported an altered differentiation processes of FT epithelial cells and an impaired ovulation
77 and oocytes spindle organization [17-19].

78 Physiological/pathological changes of FT epithelium have been found in different species as
79 rat [20], hamster [21], pig [22], goat [23] and horse [24]. Also, the ultrastructural features of
80 mucosa and epithelial cells, such as the presence, distribution, and location of secretory and
81 ciliated cells in the various portions of the human and murine FTs during the hormonal cycle
82 have been described [25, 26]. Interestingly, in mouse FTs the percentage of the ampullar
83 epithelial cells and their proliferation rate were found to be estrus cycle-dependent [26].
84 Exogenous ovarian steroids, especially E2, accelerate the differentiation and maturation of
85 secretory cells in mouse FTs [27].

86 However, the effects on FT ultrastructure exerted by COH are, to our knowledge, not yet
87 investigated. Therefore, in the present study, we evaluated the ultrastructure of the ampulla,
88 the third portion of mouse FTs, following 4R and 8R of gonadotropin administration by
89 transmission (TEM) and scanning (SEM) electron microscopy.

90

91 **MATERIALS AND METHODS**

92 *Animals*

93 *Mus musculus* Swiss CD1 female adult mice (2-3-month-old; Harlan Italy, Udine,
94 Italy, $N = 15$) were housed in the animal facility under controlled temperature ($21 \pm 1^\circ\text{C}$),
95 with 12:12 h light: dark cycle and free access to food and water. All the experimental
96 procedures and the animals were maintained in accordance with national and international
97 law and policies (European Economic Community Council Directive 86/609, OJ 358, 1 Dec
98 12, 1987; Italian Legislative Decree 116/92, Gazzetta Ufficiale della Repubblica Italiana n.
99 40, Feb 18, 1992; National Institutes of Health Guide for the Care and Use of Laboratory
100 Animals, NIH publication no. 85-23, 1985). The Italian Ministry of Health and the local
101 committee (University of L'Aquila) for the animal care and use approved the experimental
102 protocols, in compliance with the accepted veterinary medical practice. Animals were
103 euthanized by cervical dislocation after an inhalant overdose of carbon dioxide (CO_2 , 10-
104 30%), followed by cervical dislocation. All efforts were made to minimize animal suffering.

105

106 ***Experimental protocols and hormonal treatments***

107 Animals in which the early luteal phase of the estrous cycle was evaluated by
108 examination of the vagina and vaginal smears ($N = 4$), and without any hyperstimulation,
109 were used as Control (Ctr). Repetitive cycles of ovarian stimulation were performed
110 according to previous studies [17, 18]. Briefly, mice ($N = 11$) were injected i.p. with 5 IU of
111 PMSG (pregnant mare serum gonadotropin) (Folligon, Milano, Italy) and after 48 h with 5
112 IU of hCG (human chorionic gonadotropin) (Corulon, Milano, Italy). The timing of four to
113 eight repeated rounds (4R, 8R) of stimulation was selected according to [17] and [18]. In
114 particular, the COH protocol (PMSG+hCG) was repeated four times in the mice of 4R group
115 ($N=6$) and eight times in those of 8R group ($N=5$). All the rounds were performed at intervals

116 of one week between each. After approximately 16 hours from the last hCG injection (in the
117 4th and 8th week respectively), mice were sacrificed as described above. From each animal,
118 both oviducts were collected, washed in PBS and used for light and electron microscopy
119 analysis.

120

121 ***Light microscopy (LM) and transmission electron microscopy (TEM)***

122 Left FTs were isolated from their neighboring ovaries, gently washed in phosphate-
123 buffered saline (PBS) solution and immediately fixed in 2.5% glutaraldehyde (Agar
124 Scientific, Cambridge Road Stansted Essex, UK)/0.1M PBS. Fixed samples were maintained
125 at 4°C for at least 48h until the next preparative for TEM [28-31]. Firstly, FTs from each
126 experimental group (Ctr, 4R, 8R) were cut into small sections to isolate the third portion, i.e.
127 the ampullae. Successively, the pieces were rinsed in PBS, post-fixed with 1% osmium
128 tetroxide (Agar Scientific, Stansted, UK)/0.1 M PBS and rinsed again in 0.1 M PBS. Samples
129 were then dehydrated in ascending series of ethanol (Carlo Erba Reagenti, Milan, Italy),
130 immersed in propylene oxide (BDH Italia, Milan, Italy) for solvent substitution and
131 embedded in epoxy resin EMbed-812 (Electron Microscopy Sciences, Hatfield, PA, USA).
132 Semithin sections (1 mm thick) were stained with Methylene Blue, examined using a light
133 microscope (LM) (Zeiss Axioskop) and photographed using a digital camera (Leica
134 DFC230). Ultrathin sections (60–80 nm) were cut with a diamond knife, on a Reichert-Jung
135 Ultracut E ultramicrotome (Reichert Technologies, Munich, Germany), mounted on copper
136 grids and contrasted with saturated uranyl acetate followed by lead citrate (SIC, Rome, Italy).
137 They were examined and photographed using Zeiss EM10 and Philips TEM CM100 Electron
138 Microscopes operating at 80 kV.

139 We evaluated the following parameters for the qualitative assessment of the ultrastructural
140 preservation of mouse oviducts: general features; morphology of the *tunicae mucosa*,
141 *muscularis* and *serosa*; membrane integrity of the cells; morphology of the nucleus,
142 chromatin, and nuclear envelope; type and quality of organelles and inclusions; configuration
143 of mitochondria; type of granules, vesicles and vacuoles; intercellular projections;
144 microvillus pattern and presence or extent of cilia [32-36].

145

146 ***Scanning electron microscopy (SEM)***

147 Ampullar samples of the right FTs were processed for conventional [37-41] and
148 variable pressure (VPSEM) SEM analysis. For each experimental group (Ctr, 4R, 8R), the
149 isolated oviducts of their neighboring ovaries were fixed in 2.5% glutaraldehyde/0.1M PBS
150 at 4°C for at least 48 h. Selected sections of ampulla were processed either for conventional
151 or VPSEM preparation. Briefly, fixed samples were washed in 0.1M PBS, post-fixed in 1%
152 osmium tetroxide (Agar Scientific, Stansted, UK)/0.1M PBS, washed again in 0.1M PBS and
153 dehydrated in ascending ethanol series (Carlo Erba Reagenti, Milan, Italy). Following critical
154 point drying in a CO₂ atmosphere (Emitech K850, Ashford, Kent, UK), samples processed
155 for conventional SEM and VPSEM analysis were mounted onto aluminum stubs and coated
156 with platinum (4 nm in thickness) (Emitech K550 sputter coater, Ashford, Kent, UK). The
157 observations were performed at a low accelerating voltage (5-10kV in conventional SEM
158 (Hitachi S-4000) and at higher accelerating voltage (15kV) in VPSEM (Hitachi SU 3500)
159 [32, 35, 42, 43].

160

161 ***Morphometric analysis***

162 The ImageJ software (<http://rsbweb.nih.gov/ij/>) was used to measure the numerical
163 density and dimension of normal and damaged mitochondria from columnar epithelial cells
164 (CECs) of the *tunica mucosa* on low-magnification TEM micrographs of Ctr, 4R and 8R
165 groups. The numerical density of mitochondria was expressed as number of organelle per
166 100 μm^2 of epithelial area [44]. Mitochondria were classified, according to their
167 ultrastructural appearance, in: i) normal, i.e. intact, with round/elongated shape, with
168 electron-dense lamellar cristae; ii) damaged, with either swollen, irregular, or deficient
169 cristae; patchy or degenerated matrix and evident breaks in the wall of mitochondrial
170 membrane. The quantity/plethora of normal and damaged mitochondria per group was also
171 expressed as percentage of total mitochondria numerical density. For each experimental
172 group, at least three sections from three different experiments were selected for the
173 morphometric analysis.

174

175 ***Statistical analysis***

176 Dimension and numerical density of normal and damaged mitochondria were
177 expressed as mean \pm standard deviation (SD). Statistical comparisons were performed using
178 one-way ANOVA with Tukey's honest significant difference (HSD) tests for post-hoc
179 analysis (GraphPad InStat. GraphPad Software, La Jolla, USA). Differences in values were
180 considered significant if $P < 0.05$.

181

182 **RESULTS**

183 ***Control group***

184 By LM, the *tunica mucosa* of the ampullar region of FTs was folded in many branches
185 projecting into the lumen and constituted by columnar epithelial cells (CECs), ciliated (CCs)
186 and non-ciliated (NCCs) (Fig. 1A). Cuboidal cells were also found. CCs showed less intense
187 staining than the secretory NCs. The CECs presented integral nuclei delimited by an evident
188 nuclear membrane. The *tunica muscularis* showed the characteristic orientation of smooth
189 muscle fibers, arranged in two usually well-defined layers (Fig. 1A). In particular, the outer
190 layer showed individual fiber bundles oriented in a longitudinal plane while the inner one
191 was made of circular fibers. The *tunica serosa*, the external most layer, was made of a
192 squamous mesothelium and an underlying subtle rim of connective tissue (Fig. 1A).

193 The TEM analysis of the FT epithelium showed that nuclei were roundish-to-amoeboid in
194 shape, delimited with a continuous and electron-dense nuclear membrane often indented,
195 (Fig. 1B). Inside the nucleus, the chromatin appeared abundant and uniformly distributed or,
196 occasionally, with heterochromatin clustered in clumps or located as marginal patches under
197 the nuclear membrane (Fig. 1B). In the cytoplasm, numerous round and elongated
198 mitochondria with electron-dense lamellar cristae were visible and interspersed with those
199 characterized by an electron-pale content. Mitochondria were often found in association with
200 thin endoplasmic reticulum (ER) tubules and/or networks (Figs. 1B-1D). Highly electron-
201 dense secondary lysosomes and multivesicular bodies were frequently detected (Fig. 1C).

202 Lipid droplets (Fig. 1B) and Golgi apparatus were rarely found scattered throughout the CEC
203 cytoplasm. The cytoplasm also contained moderate electron-dense aggregates of glycogen
204 particles (Fig. 1C, 1E). Electron-negative vacuoles were rarely seen. CCs appeared electron-
205 lucent with motile cilia protruding into the lumen. They consisted of an evident axoneme of
206 nine peripheral doublet microtubules, surrounding a central complex with two central

207 microtubules and the central sheath (9 + 2 arrangement) (Figs. 1E). Among the cilia,
208 numerous long and thin microvilli were also evident (Figs. 1B-E). The luminal side of CCs
209 contained the typical cylindric basal bodies, located in rows immediately beneath the cell
210 membrane (Fig. 1E). NCs showed apical protrusions with numerous short and long
211 microvilli, usually continuous; occasionally, areas with rare microvilli were detected (Figs.
212 1C, 1D). It was also noticed the presence of dense secretory granules (Figs. 1C, 1D).
213 Junctional complexes between neighboring epithelial cells were well developed (1B).
214 Usually, adjacent epithelial cells were connected by apical *zonulae occludens*, followed by
215 *zonulae adhaerens* (Figs. 1B, 1D).

216

217 **4 ROUNDS**

218 After 4R of COH, the *tunica mucosa* of FTs was folded and highly branched, as seen
219 by LM. The epithelium, as in the control group, was made by a single layer of cuboidal or
220 columnar cells, whose round/ovoid nuclei were intensely stained (Fig. 2A). Both the outer
221 and the inner layers of the *tunica muscularis* were visible in transversal sections (Fig. 2A).
222 The *tunica serosa* did not show any difference in respect to controls (Fig. 2A).
223 The ultrastructural analysis by TEM showed single-layered CECs with round-to-ovoidal
224 nuclei delimited by an uninterrupted electron-dense nuclear membrane. Irregularly shaped
225 nuclei showed a marginal organization of electron-dense heterochromatin, sometimes
226 organized in highly condensed patches, with occasionally dense nucleoli (Figs. 2B-2E). In
227 the cytoplasm, round/elongated and electron-dense mitochondria were found together with
228 abundant severely swollen mitochondria, characterized by a pale and marginalized content,
229 degenerated matrix and a few or damaged cristae (Figs. 2B-2F). Numerous electron-negative

230 vesicles were observed and, at high magnification, most of them were autophagosomes
231 containing degraded mitochondria (Fig. 2E and *inset*). Prominent intracytoplasmic vacuoles
232 lined by microvilli were occasionally detected, presumably corresponding to
233 intracytoplasmic pouches of the plasma membrane (Fig. 2F). Multivesicular bodies with
234 large vesicles, high electron-dense secondary lysosomes, ER tubular elements, and lipid
235 droplets were also found (Figs. 2B, 2D). Small elements of the Golgi complex and glycogen
236 accumulations were rarely detected (not shown). Among CECs, intercellular junctions were
237 well preserved and organized as in controls (Figs. 2B, 2C). The microvillar distribution
238 pattern in NCs did not show evident variations, respect to those seen in the control group.
239 However, areas with rare microvilli were occasionally found (Fig. 2B, 2C). In the observed
240 sections, CCs were not found.

241

242 **8 ROUNDS**

243 After 8R, the *tunica mucosa* and *tunica muscularis* did not appear different respect to
244 the previous groups, as seen by LM (Fig. 3A). The nuclei of CECs from the highly folded
245 *tunica mucosa* and the two layers of *tunica muscularis* were detected, as previously described
246 (Fig. 3A). The *tunica serosa*, when visible in section, did not show any difference in respect
247 to the previous groups (Fig. 3A).

248 TEM analysis showed that the general ultrastructure of nuclei, lipid droplets, ER
249 tubules/networks, Golgi apparatus, secondary lysosomes, multivesicular bodies, microvilli
250 and intercellular connections was similar between 4R and 8R (Figs. 3B-3F). Similarly to the
251 4R group, the most evident and peculiar morphological alterations affected the mitochondria.
252 Mitochondrial damages were observed more frequently respect to 4R. They ranged from a

253 severely swollen appearance up to a disrupted aspect with electron-negative content and
254 partial or complete cristolysis (Fig. 3C). The matrix of swollen mitochondria appeared
255 patchy, and often, the mitochondrial membrane presented evident breaks in the wall (Figs.
256 3B-3D). Mitochondria showing a partly swollen aspect, with some area of still dense matrix,
257 were also found together with a few rounds/elongated normal electron-dense mitochondria
258 with lamellar cristae (Fig. 3B). Mitophagic vacuoles were often close to lysosomes or
259 multivesicular bodies (3E). Secretory granules, with an electron-dense homogeneous
260 content, appeared beneath the cell surface facing the lumen in NCs (Fig. 3F). Coated vesicles
261 were occasionally detected as in the 4R group; CCs with cilia projecting into the lumen and
262 glycogen accumulations were not found in the observed sections.

263

264 ***Surface Ultrastructural Analysis by SEM***

265 Representative micrographs of CECs of *tunica mucosa* from the ampullar region of
266 FTs taken by conventional SEM (Figs. 4A-4C) and VPSEM (Fig. 4D) were selected. A
267 panoramic micrograph showed tufts of cilia nonuniformly distributed in the surface of CCs,
268 protruding into the lumen and surrounded by short microvillar projections of NCs (Fig. 4A,
269 control group). At higher magnification, a single tuft of cilia appeared well preserved (Fig.
270 4B, control group). Numerous microvilli densely covered the NCs surface. They were long
271 and homogeneous (Fig. 4C, 4R group) or short and not homogeneously distributed (Fig. 4D,
272 4R group).

273

274 ***Morphometric analysis***

275 Morphometric analysis revealed that the dimension (expressed as mean \pm SD) of
276 normal mitochondria per 100 μm^2 was $0.444 \pm 0.096 \mu\text{m}$ in Ctr, $0.415 \pm 0.060 \mu\text{m}$ in 4R and
277 $0.472 \pm 0.086 \mu\text{m}$ in 8R, without significant variations among groups ($P>0.05$) (table 1).
278 When dimension was measured in damaged mitochondria, we found a significant increase
279 after 4R ($0.553 \pm 0.118 \mu\text{m}$ vs. $0.659 \pm 0.099 \mu\text{m}$; $P<0.05$) and 8R ($0.553 \pm 0.118 \mu\text{m}$ vs.
280 $0.817 \pm 0.179 \mu\text{m}$; $P<0.001$). This increase was significant also between treated groups
281 ($0.659 \pm 0.099 \mu\text{m}$ vs. $0.817 \pm 0.179 \mu\text{m}$, 4R vs. 8R respectively; $P < 0.001$) (table 1).
282 The numerical density of normal mitochondria dramatically decreased after 4R and 8R,
283 respect to Ctr group (5.3 ± 0.5 and 9.6 ± 4.1 vs. 40 ± 12.1 , respectively; $P < 0.01$), with no
284 significant variation among treated groups ($P>0.05$) (table 1).
285 Concomitantly, the density of damaged mitochondria significantly increased after 4R,
286 respect to controls (57.6 ± 7.3 vs. 22.3 ± 2.3 , respectively; $P<0.01$); however, after 8R the
287 increase was not significant respect to controls (33 ± 7.8 vs. 22.3 ± 2.3 , respectively; $P > 0.05$)
288 (Table 1).
289 Quantification of the frequency of damaged mitochondria among groups revealed that their
290 percentage significantly increased after 4R, by reaching the highest values, and less after 8R
291 ($36.665 \pm 7.629 \%$, $91.45 \pm 1.41 \%$, $78.103 \pm 4.405 \%$, CTR vs. 4R vs. 8R, respectively; P
292 < 0.05) (Table 1).

293

294 **DISCUSSION**

295 Gonadotropins are used for COH but their effects after repeated cycles of
296 hyperstimulation on the ampullar epithelium of FTs have not yet investigated from an
297 ultrastructural point of view. We found that, after 4R and 8R, the *tunicae mucosa* and

298 *muscularis* of mouse FTs appeared well-preserved by LM with no evident signs of
299 morphological alterations, as in other mammals [45, 46]. The ultrastructural analysis of CECs
300 by TEM showed, in all groups, the presence of well-preserved nuclei and cell junctions, lipid
301 droplets, ER tubules/networks, Golgi apparatuses, secondary lysosomes, multivesicular
302 bodies and microvilli, in accordance with the literature describing the physiological
303 morphology of oviducts [23, 24, 27]. However, electron microscopy evidenced specific
304 changes affecting mitochondria and cilia of the CECs of the mucosa layer, especially after
305 8R.

306 Literature data show that repeated rounds of hyperstimulation may affect at a different extent
307 the female reproductive tracts by inducing a decrease in the pregnancy rates from 25.2% to
308 17.8% after the 4R, and up to 11.2 % after more than 12R [47]. This can be accounted for
309 significant changes in oocyte and follicular quality, as well as for the reduced developmental
310 potential of embryos [17, 19, 48, 49]. In particular, after 4R there were observed a decrease
311 in the percentage of mouse oocytes with a uniform distribution of mitochondria, an increase
312 in the aggregation of the Golgi apparatus and endoplasmic reticulum, and the induction of
313 spindle disruption [49]. However, in a recent study on women stimulated by a standard
314 antagonist protocol, no adverse effects were found after repeated cycles of COH. At 3R or
315 more the number of mature oocytes, zygotes and clinical pregnancy rates were even higher
316 than those obtained by 2R or less [50]. These contrasting results could be accounted for the
317 milder stimulation used and for a different specie-specific sensitivity that deserves to be
318 better addresses.

319 Repeated cycles of COH were also connected to oxidative stress. In fact, while ROS
320 production augmented after 4R of COH, the *Oct4* transcripts started to decrease [49]. This is

321 in agreement with our previous data, showing a progressive reduction of the protein OCT3/4
322 from 4 to 8R in mouse [18]. Moreover, oxidative damages were also detected in mouse
323 ovaries. The oxidative damage, including an increased content of 8-OH-dG, lipid peroxides
324 and protein carbonyls, positively correlated with the number of COH cycles [51]; it induced
325 mitochondrial abnormalities and a decrease in antioxidants compatible with ovarian aging
326 [52]. The effects of COH were determined also in mouse cumulus cells, where the mtDNA
327 copy number decreased as the number of stimulation increased, together with altered DNA
328 methylation in nuclear-encoded DNA polymerase gamma A (PolgA) and consequent
329 changes in PolgA expression [53]. Moreover, mRNA expression levels of cytochrome b
330 (CYTB), cytochrome c oxidase subunit 1 (COX1), NADH dehydrogenase subunit (ND4),
331 and NADH dehydrogenase subunit 2 (ND2), all encoded by mtDNA, were altered following
332 repeated superovulation in cumulus cells [53]. Detrimental effects of repeated cycles of COH
333 on mitochondria were seen by the reduction of ATP production on GV-stage mouse oocytes
334 matured *in vitro* after four rounds [54].

335 These adverse effects on the mitochondrial function after superovulation in oocytes, cumulus
336 cells and embryos [44, 48, 49], prompted us to focus on the ultrastructure of mitochondria
337 dispersed in the columnar epithelial cells of FTs. Interestingly, it was found the presence of
338 numerous swelled or even disrupted elements, most of them undergoing to phenomena of
339 mitophagy, evident already after 4 repeated cycles, in agreement to a previous study in rabbit
340 oviducts after hCG injection [55]. These ultrastructural alterations of CEC mitochondria due
341 to COH, in agreement with the above reported findings, can be probably responsible for a
342 hampered energetic support of the oviductal epithelium [56, 57]. Moreover, the presence of
343 reduced storage of glycogens after repeated cycles of COH, respect to controls, can further

344 sustain the hypothesized energetic imbalance at a time where it is expected the fertilized egg
345 to be in the FTs and in need of the proper enzymes and nutrients for growth and survival [58-
346 60].

347 Reactive oxygen species (ROS) are present in the FT fluids [61]. Raised levels of ROS are
348 responsible for aberrations in the tubal environment which result in infertility [62]. We could,
349 therefore, speculate that repeated cycles of COH in FTs could alter hormonal imbalance,
350 inducing stressful condition with the increase of ROS and the reduction of endogenous
351 antioxidants. ROS, as the nitric oxide (NO), have a relaxing effect on the tubal smooth
352 musculature at physiological concentrations but displayed a cytotoxic action when their
353 levels increase [62]. Some isoform of the NO synthase (NOS) is upregulated by hormones
354 and gonadotropins (LH/hCG), thus increasing NO production [63]; this could probably occur
355 after repeated cycles of COH. Furthermore, the mitochondrial manganese superoxide
356 dismutase (Mn-SOD) of epithelial cells is involved in mitigating oxygen toxicity to ovulated
357 oocytes and developing embryos in the FT. Its reduction induces a redox imbalance and
358 subsequent mitochondrial damage, as evidenced by swelling, vacuolization or barely
359 visible cristae found here and by others [61].

360 The morphometric analysis evidenced that, after 4R onwards of COH, there was a significant
361 increase in the frequency and density of damaged mitochondria from the oviductal
362 epithelium, thus strengthening the ultrastructural observations described [55-57]. The slight
363 improvement observed in terms of density and frequency of damaged mitochondria at 8R,
364 respect to 4R, could be probably due to cytoplasmic remodeling mechanisms activated by
365 the oxidative damage, that may establish domains of autonomous regulation of mitochondrial
366 function and activity, as previously reported in mammalian oocytes and embryos [44, 64].

367 The mitochondrial dysfunction here observed may, probably, be connected to the absence of
368 ciliated epithelium in the sections observed, as the fibrils' tips during ciliogenesis are laterally
369 connected to mitochondria [65]. Malfunction of the ciliary beat impairs the laminar fluid flow
370 above the FT epithelia, thus likely reducing the clearance of oxidative stress caused by
371 follicular fluid after ovulation [66].

372 In mouse oviducts, CCs can be rise from NCs under the direction of ovarian steroids [67,
373 68]. As recently seen in bovine, at least seven types of cells at different
374 translational/transcriptional states of ciliogenesis are present in the oviductal epithelium, and
375 their numbers are regulated by the estrous cycle [69]. This might provide the optimal
376 environment for gamete transport, fertilization and embryo development [69]. The fine
377 tuning of the histoarchitecture of FTs could be particularly sensitive to excessive estrogens
378 induced by COH. After mild stimulation, an increased proliferation was, in fact, observed
379 within the tubal epithelium, with pseudostratification of the epithelial cells and loss of their
380 ciliated border [70]. Increased proliferation and multilayering of the tubal epithelium with
381 the appearance of a micropapillary pattern were frequently observed at higher doses of
382 gonadotropins [70].

383 FT epithelial cells expressed both estrogen and progesterone receptors, that were down-
384 regulated by treatment with exogenous steroids [70, 71]. However, while membrane steroid-
385 binding proteins (as membrane progestin receptors) are exclusively expressed in CCs of mice
386 and women - to probably control the beating of the cilia or receptor expression via feedback
387 systems [71] - the nuclear Progesterone Receptor (PGR) is immunolocalized also in smooth
388 muscle cells [72]. Here, high levels of progesterone or progestagens promote in the luteal
389 phase relaxation of the sphincter in the isthmus, allowing cilia to transport the pre-embryo

390 into the uterine cavity. Differently, the endogenous rise of estradiol (E2) during the
391 periovulatory period activates contractions of the myosalpinx, aiding the transport of
392 spermatozoa [73].

393 Gonadotropin receptors (FSHR and LHR) are also expressed in FTs and regulated by ovarian
394 steroids [74]. It is noteworthy that hyperstimulation with FSH downregulated FSHR present
395 in the blood and lymphatic vessels of the *tunica* mucosa as well as in the smooth muscle cells,
396 thus affecting angiogenesis, vasculogenesis and oviductal contractions. High doses of
397 eCG/hCG induced a reduction in the protein levels of LHR in the oviductal ampulla with a
398 strong impact on ampullary physiology and function, as glycoprotein synthesis and secretion
399 [75].

400 The findings obtained from this study may corroborate to the harmful side-effects of the
401 ovarian hyperstimulation in regard to the maintenance of cellular integrity and strengthen the
402 aspect that increased rounds can contribute to the risk of developing gynecological cancers
403 [5, 76]. Endometrial biopsies retrieved from cycling IVF patients, with at least three repeated
404 IVF cycles with no pregnancy, revealed a lower expression of the tumor suppressor p27 and
405 a higher expression of its ligase S-phase kinase-interacting protein-2 (Skp2), compared to
406 non-stimulated normal cycling women [77]. Moreover, in the 25% of patients of the study
407 group, Skp2 expression reached concentrations demonstrated in endometrial carcinoma.
408 These findings suggested that repeated hormone stimulation cycles may disrupt endometrial
409 physiology, potentially towards abnormal proliferation [77]. In fact, it has been found that
410 gonadotropin stimulation could produce tubal and ovarian histopathologic abnormalities with
411 a dose-effect [78]. Moreover, the oviducts were reported to be the origin of OC as the high-
412 grade intraepithelial serous carcinoma and ovarian carcinosarcoma [79, 80], thus making the

413 tubal ligation and hysterectomy methods of choice in reducing the possibility for OC
414 development [81, 82].

415 In conclusion, the ultrastructural alterations found in mitochondria and ciliar coverage of the
416 mouse FT epithelium after repeated rounds of hyperstimulation, further demonstrate that
417 COH has a detrimental impact on CECs morphology. Due to the role of FTs in ensuring
418 fertilization and the subsequent transport of the embryo in the uterus, ultrastructural
419 alterations here described may also contribute to infertility.

420

421

422 **Conflict of interest**

423 The authors declare that they have no competing interests.

424

425 **Author contribution statement:** SBi, SC, MGP and GM conceived the study; SBi, GR and
426 SBe treated the animals and collected the samples; SA, MGP and MB performed TEM and
427 SEM experiments and analyzed data; SA and MGP wrote the paper; GM, SAN and SC
428 analyzed data and revised the manuscript; GF, SBi and MAK critically revised the
429 manuscript. All the authors accepted the final version of the manuscript.

430

431 **Acknowledgments:** The authors thank Mr. Ezio Battaglione, Laboratory for Electron
432 Microscopy “Pietro M. Motta”, Rome, and Miss Aurora Navicella, Laboratory of
433 Biotechnologies of Reproduction, University of L’Aquila. Funds for this study were provided
434 by Departmental grants from the Dept. of Life, Health and Environmental Sciences,
435 University of L’Aquila (RIA, Prof. Guido Macchiarelli and Prof. Sandra Cecconi) and the

436 Department of Anatomy, Histology, Forensic Medicine and Orthopaedics, La Sapienza

437 University of Rome (University grants, Prof. Stefania Annarita Nottola).

438

439

440 **REFERENCES**

- 441 1. **Mahe JY, Christianson MS.** Controlled ovarian stimulation and triggers in in vitro
442 fertilization: protocol personalization key to optimize outcomes. *Minerva Endocrinol*
443 2018; **43**: 37-49.
- 444 2. **Fauser BC, Devroey P.** Reproductive biology and IVF: ovarian stimulation and luteal
445 phase consequences. *Trends in Endocrinology and Metabolism* 2003; **14**: 236-242.
- 446 3. **El Tokhy O, Kopeika J, El-Toukhy T.** An update on the prevention of ovarian
447 hyperstimulation syndrome. *Women's Health* 2016; **12**: 496-503.
- 448 4. **Adda-Herzog E, Poulain M, de Ziegler D, Ayoubi JM, Fanchin R.** Premature
449 progesterone elevation in controlled ovarian stimulation: to make a long story short. *Fertil*
450 *Steril* 2018; **109**: 563-570.
- 451 5. **Kroener L, Dumesic D, Al-Safi Z.** Use of fertility medications and cancer risk: a review
452 and update. *Curr Opin Obstet Gynecol* 2017; **29**: 195-201.
- 453 6. **Del Pup L, Peccatori FA, Levi-Setti PE, Codacci-Pisanelli G, Patrizio P.** Risk of
454 cancer after assisted reproduction: a review of the available evidences and guidance to
455 fertility counselors. *Eur Rev Med Pharmacol Sci.* 2018; **22**(22): 8042-8059.
- 456 7. **Rizzuto I, Behrens RF, Smith LA.** Risk of ovarian cancer in women treated with
457 ovarian stimulating drugs for infertility. *Cochrane Database Syst Rev.* 2019; **6**:
458 CD008215.
- 459 8. **Cakmak H, Rosen MP.** Ovarian stimulation in cancer patients. *Fertil Steril* 2013; **99**:
460 1476-1484.
- 461 9. **Diergaarde B, Kurta ML.** Use of fertility drugs and risk of ovarian cancer. *Curr Opin*
462 *Obstet Gynecol.* **26**; 2014: 125-129.

- 463 10. **Verhage HG, Mavrogianis PA, Boice ML, Li W, Fazleabas AT.** Oviductal epithelium
464 of the baboon: hormonal control and the immuno-gold localization of oviduct-specific
465 glycoproteins. *Am J Anat* 1990; **187**: 81-90.
- 466 11. **Wessel T, Schuchter U, Walt H.** Ciliary motility in bovine oviducts for sensing rapid
467 non-genomic reactions upon exposure to progesterone. *Horm Metab Res.* 2004; **36**; 136-
468 141.
- 469 12. **Carretero A, Ruberte J, Navarro M.** Female genital organs. In *Morphological Mouse*
470 *Phenotyping: Anatomy, Histology and Imaging*, edn 1. Eds J Ruberte, A Carretero, M
471 Navarro. Academic Press Inc.; 2017: 227-252.
- 472 13. **Lyons RA, Saridogan E, Djahanbakhch O.** The reproductive significance of human
473 Fallopian tube cilia. *Hum Reprod Update* 2006; **12**: 363-372.
- 474 14. **Paltieli Y, Eibschitz I, Ziskind G, Ohel G, Silbermann M, Weichselbaum A.** High
475 progesterone levels and ciliary dysfunction-a possible cause of ectopic pregnancy. *J Assist*
476 *Reprod Genet* 2000; **17**: 103-106.
- 477 15. **Winuthayanon W, Hewitt SC, Korach KS.** Uterine epithelial cell estrogen receptor
478 alpha-dependent and -independent genomic profiles that underlie estrogen responses in
479 mice. *Biol Reprod* 2014; **91**: 110.
- 480 16. **Zhao W, Zhu Q, Yan M, Li C, Yuan J, Qin G, Zhang J.** Levonorgestrel decreases
481 cilia beat frequency of human fallopian tubes and rat oviducts without changing
482 morphological structure. *Clin Exp Pharmacol Physiol* 2015; **42**: 171-178.
- 483 17. **Di Luigi G, Rossi G, Castellucci A, Leocata P, Carta G, Canipari R, Nottola SA,**
484 **Cecconi S.** Repeated ovarian stimulation does not affect the expression level of proteins

- 485 involved in cell cycle control in mouse ovaries and fallopian tubes. *J Assist Reprod Genet*
486 2014; **31**: 717-724.
- 487 18. **Di Nisio V, Rossi G, Palmerini MG, Macchiarelli G, Tiboni GM, Cecconi S.** Increased
488 rounds of gonadotropin stimulation have side effects on mouse fallopian tubes and
489 oocytes. *Reproduction* 2018; **155**: 245-250.
- 490 19. **Van Blerkom J, Davis P.** Differential effects of repeated ovarian stimulation on
491 cytoplasmic and spindle organization in metaphase II mouse oocytes matured in vivo and
492 in vitro. *Hum Reprod* 2001; **16**: 757-764.
- 493 20. **Yang J, Chi C, Liu Z, Yang G, Shen ZJ, Yang XJ.** Ultrastructure damage of oviduct
494 telocytes in rat model of acute salpingitis. *J Cell Mol Med* 2015; **19**: 1720-1728.
- 495 21. **El-Mestrah M, Kan FW.** Ultrastructural and ultracytochemical features of secretory
496 granules in the ampullary epithelium of the hamster oviduct. *Anat Rec* 1999; **255**: 227-
497 239.
- 498 22. **Katarzyna SM, Wiesław B, Anna R.** The tunica mucosa of the oviduct in case of
499 ovarian cysts presence in sows. *Folia Histochem Cytobiol* 2010; **48**: 148-156.
- 500 23. **Sharma RK, Singh R, Bhardwaj JK.** Scanning and transmission electron microscopic
501 analysis of ampullary segment of oviduct during estrous cycle in caprines. *Scanning* 2015;
502 **37**: 36-41.
- 503 24. **Desantis S, Zizza S, Accogli G, Acone F, Rossi R, Resta L.** Morphometric and
504 ultrastructural features of the mare oviduct epithelium during oestrus. *Theriogenology*
505 2011; **75**: 671-678.

- 506 25. **Barberini F, Makabe S, Correr S, Luzi A, Motta PM.** An ultrastructural study of
507 epithelium differentiation in the human fetal fallopian tube. *Acta Anatomica (Basel)* 1994;
508 **151:** 207-219.
- 509 26. **Morita M, Miyamoto H, Sugimoto M, Sugimoto N, Manabe N.** Alterations in cell
510 proliferation and morphology of ampullar epithelium of the mouse oviduct during the
511 estrous cycle. *J Reprod Dev* 1997; **43:** 235-241.
- 512 27. **Lauschova I.** Secretory cells and morphological manifestation of secretion in the mouse
513 oviduct. *Scripta Medica* 2003; **76:** 203-214.
- 514 28. **Palmerini MG, Nottola SA, Leoni GG, Succu S, Borshi X, Berlinguer F, Naitana S,**
515 **Bekmukhambetov Y, Macchiarelli G.** In vitro maturation is slowed in prepubertal lamb
516 oocytes: ultrastructural evidences. *Reproductive Biology and Endocrinology* 2014; **12:**
517 115.
- 518 29. **Leoni GG, Palmerini MG, Satta V, Succu S, Pasciu V, Zinellu A, Carru C,**
519 **Macchiarelli G, Nottola SA, Naitana S, Berlinguer F.** Differences in the Kinetic of
520 the First Meiotic Division and in Active Mitochondrial Distribution between Prepubertal
521 and Adult Oocytes Mirror Differences in their Developmental Competence in a Sheep
522 Model. *PLoS One* 2015; **10:** e0124911.
- 523 30. **Coticchio G, Dal Canto M, Fadini R, Mignini Renzini M, Guglielmo MC, Miglietta**
524 **S, Palmerini MG, Macchiarelli G, Nottola SA.** Ultrastructure of human oocytes after in
525 vitro maturation. *Mol Hum Reprod* 2016; **22:** 110-118.
- 526 31. **Khalili MA, Shahedi A, Ashourzadeh S, Nottola SA, Macchiarelli G, Palmerini MG.**
527 Vitriification of human immature oocytes before and after in vitro maturation: a review. *J*
528 *Assist Reprod Genet* 2017; **34:** 1413-1426.

- 529 32. **Nottola SA, Cecconi S, Bianchi S, Motta C, Rossi G, Continenza MA, Macchiarelli**
530 **G.** Ultrastructure of isolated mouse ovarian follicles cultured in vitro. *Reprod Biol*
531 *Endocrinol* 2011; **9**: 3.
- 532 33. **Bianchi S, Macchiarelli G, Micara G, Linari A, Boninsegna C, Aragona C, Rossi G,**
533 **Cecconi S, Nottola SA.** Ultrastructural markers of quality are impaired in human
534 metaphase II aged oocytes: a comparison between reproductive and in vitro aging. *J Ass*
535 *Reprod Genet* 2015; **32**: 1343-1358.
- 536 34. **Palmerini MG, Zhurabekova G, Balmagambetova A, Nottola SA, Miglietta S, Belli**
537 **M, Bianchi S, Cecconi S, Di Nisio V, Familiari G, Macchiarelli G.** The pesticide
538 Lindane induces dose-dependent damage to granulosa cells in an in vitro culture. *Reprod*
539 *Biol* 2017; **17**: 349-356.
- 540 35. **Palmerini MG, Belli M, Nottola SA, Miglietta S, Bianchi S, Bernardi S, Antonouli**
541 **S, Cecconi S, Familiari G, Macchiarelli G.** Mancozeb impairs the ultrastructure of
542 mouse granulosa cells in a dose-dependent manner. *J Reprod Dev* 2018; **64**: 75-82.
- 543 36. **Taghizabet N, Khalili MA, Anbari F, Agha-Rahimi A, Nottola SA, Macchiarelli G,**
544 **Palmerini MG.** Human cumulus cell sensitivity to vitrification, an ultrastructural study.
545 *Zygote* 2018; **26**: 224-231.
- 546 37. **Martelli A, Palmerini MG, Russo V, Rinaldi C, Bernabò N, Di Giacinto O,**
547 **Berardinelli P, Nottola SA, Macchiarelli G, Barboni B.** Blood vessel remodeling in pig
548 ovarian follicles during the periovulatory period: an immunohistochemistry and SEM-
549 corrosion casting study. *Reprod Biol Endocrinol* 2009; **7**: 72.
- 550 38. **Macchiarelli G, Nottola SA, Palmerini MG, Bianchi S, Maione M, Lorenzo C,**
551 **Stifano G, Di Marco E, Correr S.** Morphological expression of angiogenesis in the

552 mammalian ovary as seen by SEM of corrosion casts. *Ital J Anat Embryol* 2010; **115**: 109-
553 114.

554 39. **Macchiarelli G, Palmerini MG, Nottola SA, Cecconi S, Tanemura K, Sato E.**
555 Restoration of corpus luteum angiogenesis in immature hypothyroid rdw rats after
556 thyroxine treatment: morphologic and molecular evidence. *Theriogenology* 2013; **79**:
557 116-126.

558 40. **Palmerini MG, Nottola SA, Tunjung WA, Kadowaki A, Bianchi S, Cecconi S, Sato**
559 **E, Macchiarelli G.** EGF-FSH supplementation reduces apoptosis of pig granulosa cells
560 in co-culture with cumulus-oocyte complexes. *Biochem Biophys Res Commun.* 2016; **481**:
561 159-164.

562 41. **Bernardi S, Bianchi S, Botticelli G, Rastelli E, Tomei AR, Palmerini MG,**
563 **Continenza MA, Macchiarelli G.** Scanning electron microscopy and microbiological
564 approaches for the evaluation of salivary microorganisms behaviour on anatase titanium
565 surfaces: In vitro study. *Morphologie* 2018; **102**: 1-6.

566 42. **Nottola SA, Makabe S, Stallone T, Familiari G, Correr S, Macchiarelli G.** Surface
567 morphology of the zona pellucida surrounding human blastocysts obtained after in vitro
568 fertilization. *Arch Histol Cytol* 2005; **68**: 133-141.

569 43. **Giusti I, Bianchi S, Nottola SA, Macchiarelli G, Dolo V.** Clinical electron microscopy
570 in the study of human ovarian tissues. *EMBJ* 2019; **14**: 145-151.

571 44. **Belli M, Zhang L, Liu X, Donjacour A, Ruggeri E, Palmerini MG, Nottola SA,**
572 **Macchiarelli G, Rinaudo P.** Oxygen concentration alters mitochondrial structure and
573 function in in vitro fertilized preimplantation mouse embryos. *Hum Reprod* 2019; **34**: 601-
574 611.

- 575 45. **Abe H, Hoshi H.** Morphometric and ultrastructural changes in ciliated cells of the
576 oviductal epithelium in prolific Chinese Meishan and Large White pigs during the
577 oestrous cycle. *Reprod Domest Anim* 2008; **43**: 66-73.
- 578 46. **Tienthai P, Sajjarengpong K, Techakumphu M.** Light and scanning electron
579 microscopic studies of oviductal epithelium in Thai swamp buffalo (*Bubalus bubalis*) at
580 the follicular and luteal phases. *Reprod Dom Anim* 2009; **44**: 450-455.
- 581 47. **Homburg R, Meltcer S, Rabinson J, Scharf S, Anteby EY, Orvieto R.** Is there a limit
582 for the number of in vitro fertilization cycles for an individual patient? *Fertil Steril* 2009;
583 **91**: 1329-1331.
- 584 48. **Liang L, Xu B, Zhu G.** Effect of repeated gonadotropin stimulation on ovarian reserves
585 and proliferation of ovarian surface epithelium in mice. *Front Med China* 2009; **3**: 220-
586 226.
- 587 49. **Kalthur G, Salian SR, Nair R, Mathew J, Adiga SK, Kalthur SG, Zeegers D, Hande**
588 **MP.** Distribution pattern of cytoplasmic organelles, spindle integrity, oxidative stress,
589 octamer-binding transcription factor 4 (Oct4) expression and developmental potential of
590 oocytes following multiple superovulation. *Reprod Fertil Dev* 2016; **28**: 2027-2038.
- 591 50. **Paul LT, Atilan O, Tulay P.** The effect of repeated controlled ovarian stimulation
592 cycles on the gamete and embryo development. *Zygote* 2019; **27**: 347-349.
- 593 51. **Chao HT, Lee SY, Lee HM, Liao TL, Wei YH, Kao SH.** Repeated ovarian
594 stimulations induce oxidative damage and mitochondrial DNA mutations in mouse
595 ovaries. *Ann N Y Acad Sci* 2005; **1042**: 148-56.
- 596 52. **Miyamoto K, Sato EF, Kasahara E, Jikumaru M, Hiramoto K, Tabata H,**
597 **Katsuragi M, Odo S, Utsumi K, Inoue M.** Effect of oxidative stress during repeated

598 ovulation on the structure and functions of the ovary, oocytes, and their mitochondria.
599 *Free Radic Biol Med* 2010; **49**: 674-681.

600 53. **Xie JK, Wang Q, Zhang TT, Yin S, Zhang CL, Ge ZJ.** Repeated superovulation may
601 affect mitochondrial functions of cumulus cells in mice. *Sci Rep* 2016; **6**: 31368.

602 54. **Combelles CM, Albertini DF.** Assessment of oocyte quality following repeated
603 gonadotropin stimulation in the mouse. *Biol Reprod* 2003; **68**: 812-821.

604 55. **Bondi AM, Gabrielli MG, Marchetti L, Materazzi G, Menghi G.** Cytomorphological
605 changes in the rabbit oviductal epithelium after human chorionic gonadotropin treatment.
606 *Histol Histopathol* 1997; **12**: 135-146.

607 56. **Maillo V, Sánchez-Calabuig MJ, Lopera-Vasquez R, Hamdi M, Gutierrez-Adan**
608 **A, Lonergan P, Rizos D.** Oviductal response to gametes and early embryos in
609 mammals. *Reproduction* 2016; **152**: R127-141.

610 57. **Leese HJ, Sturmey RG, Whitear S-L.** The Oviductal Environment and Early Embryo
611 Development: A Question of Supply and Demand. *Biol Reprod* 2009; **81**: 57.

612 58. **Schulte BA, Rao KP, Kreutner A, Thomopoulos GN, Spicer SS.** Histochemical
613 examination of glycoconjugates of epithelial cells in the human fallopian tube. *Lab*
614 *Invest* 1985; **52**: 207-219.

615 59. **Leese HJ, Baumann CG, Brison DR, McEvoy TG, Sturmey RG.** Metabolism of the
616 viable mammalian embryo: quietness revisited. *Mol Hum Reprod* 2008; **14**: 667-672.

617 60. **Li S, Winuthayanon W.** Oviduct: roles in fertilization and early embryo development.
618 *J Endocrinol* 2017; **232**: R1-R26.

619 61. **Tamate K, Sengoku K, Ishikawa M.** The role of superoxide dismutase in the human
620 ovary and fallopian tube. *J Obstet Gynaecol* 1995; 1995; **21**: 401-409.

- 621 62. **Agarwal A, Aponte-Mellado A, Premkumar BJ, Shaman A, Gupta S.** The effects of
622 oxidative stress on female reproduction: a review. *Reprod Biol Endocrinol* 2012; **10**: 49.
- 623 63. **Fujii J, Iuchi Y, Okada F.** Fundamental roles of reactive oxygen species and
624 protective mechanisms in the female reproductive system. *Reprod Biol Endocrinol*
625 2005; **3**: 43.
- 626 64. **Van Blerkom J.** Mitochondria in early mammalian development. *Semin Cell Dev Biol*
627 2009; **20**: 354-364.
- 628 65. **Hagiwara H.** Electron microscopic studies of ciliogenesis and ciliary abnormalities in
629 human oviduct epithelium. *Ital J Anat Embryol* 1995; **100**: 451-459.
- 630 66. **Coan M, Rampioni Vinciguerra GL, Cesaratto L, Gardenal E, Bianchet R, Dassi**
631 **E, Vecchione A, Baldassarre G, Spizzo R, Nicoloso MS.** Exploring the Role of
632 Fallopian Ciliated Cells in the Pathogenesis of High-Grade Serous Ovarian Cancer. *Int J*
633 *Mol Sci* 2018; 19.
- 634 67. **Ghosh A, Syed SM, Tanwar PS.** In vivo genetic cell lineage tracing reveals that
635 oviductal secretory cells self-renew and give rise to ciliated cells. *Development* 2017;
636 **144**: 3031-3041.
- 637 68. **Chang YH, Ding DC, Chu TY.** Estradiol and Progesterone Induced Differentiation
638 and Increased Stemness Gene Expression of Human Fallopian Tube Epithelial Cells. *J*
639 *Cancer* 2019; **10**: 3028-3036.
- 640 69. **Ito S, Yamamoto Y, Kimura K.** Analysis of ciliogenesis process in the bovine oviduct
641 based on immunohistochemical classification. *Mol Biol Rep* 2020; **47**:1003-1012.

- 642 70. **Moussa M and Farouk SM.** Ovarian stimulation induces high expression of
643 interleukin-1 β and disrupts the histological features of the fallopian tube. *Turk J Vet*
644 *Anim Sci* 2019; **43**: 186-196.
- 645 71. **Nutu M, Weijdegård B, Thomas P, Thurin-Kjellberg A, Billig H, Larsson DG.**
646 Distribution and hormonal regulation of membrane progesterone receptors beta and
647 gamma in ciliated epithelial cells of mouse and human fallopian tubes. *Reprod Biol*
648 *Endocrinol* 2009; **7**:89.
- 649 72. **Okada A, Ohta Y, Inoue S, Hiroi H, Muramatsu M, Iguchi T.** Expression of
650 estrogen, progesterone and androgen receptors in the oviduct of developing, cycling and
651 pre-implantation rats. *J Mol Endocrinol* 2003; **30**: 301-315.
- 652 73. **Wånggren K, Stavreus-Evers A, Olsson C, Andersson E, Gemzell-Danielsson K.**
653 Regulation of muscular contractions in the human Fallopian tube through prostaglandins
654 and progestagens. *Hum Reprod* 2008; **23**: 2359-2368.
- 655 74. **Gawronska B, Stepień A, Ziecik AJ.** Effect of estradiol and progesterone on oviductal
656 LH-receptors and LH-dependent relaxation of the porcine oviduct. *Theriogenology*
657 2000; **53**: 659-672.
- 658 75. **Malysz-Cymborska I, Andronowska A.** Downregulation of LH and FSH receptors
659 after hCG and eCG treatments in the porcine oviduct. *Domest Anim Endocrinol* 2016;
660 **57**: 48-54.
- 661 76. **Sanner K, Conner P, Bergfeldt K, Dickman P, Sundfeldt K, Bergh T, Hagenfeldt K,**
662 **Janson PO, Nilsson S, Persson I.** Ovarian epithelial neoplasia after hormonal infertility
663 treatment: long-term follow-up of a historical cohort in Sweden. *Fertil Steril* 2009; **91**:
664 1152-1158.

- 665 77. **Lahav-Baratz S, Koifman M, Sabo E, Auslender R, Dirnfeld M.** p27 and its
666 ubiquitin ligase Skp2 expression in endometrium of IVF patients with repeated
667 hormonal stimulation. *Reprod Biomed Online* 2016; **32**: 308-315.
- 668 78. **Lacoste CR, Clemenson A, Lima S, Lecointre R, Peoc'h M, Chene G.** Tubo-ovarian
669 dysplasia in relationship with ovulation induction in rats. *Fertil Steril* 2013; **99** 1768-1773.
- 670 79. **See SHC, Behdad A, Maniar KP, Blanco LZ Jr.** Ovarian Carcinosarcoma and
671 Concurrent Serous Tubal Intraepithelial Carcinoma With Next-Generation Sequencing
672 Suggesting an Origin From the Fallopian Tube. *Int J Surg Pathol* 2019; **27**: 574-579.
- 673 80. **Soong TR, Howitt BE, Horowitz N, Nucci MR, Crum CP.** The fallopian tube,
674 "precursor escape" and narrowing the knowledge gap to the origins of high-grade serous
675 carcinoma. *Gynecol Oncol* 2019; **152**: 426-433.
- 676 81. **Cibula D, Widschwendter M, Zikan M, Dusek L.** Underlying mechanisms of ovarian
677 cancer risk reduction after tubal ligation. *Acta Obstet Gynecol Scand* 2011; **90**: 559-563.
- 678 82. **Rice MS, Murphy MA, Vitonis AF, Cramer DW, Titus LJ, Tworoger SS, Terry KL.**
679 Tubal ligation, hysterectomy and epithelial ovarian cancer in the New England Case-
680 Control Study. *Int J Cancer* 2013; **133**: 2415-2421.
- 681
- 682

683 **LEGEND TO FIGURES**

684 **Figure 1. Control group. A.** Representative LM picture of a transversal section of mouse
685 ampulla showing the three layers of *tunica mucosa* (TM), *muscularis* (TMu) and *serosa* (TS).
686 The TM appears regularly folded and characterized by adjacent columnar epithelial cells
687 (CEC) with evident nuclei (*). In the *tunica muscularis* (TMu), the two well-defined outer
688 and inner layers are evident. The former is organized in individual smooth muscle fiber
689 bundles longitudinally oriented while the latter is organized in circular fibers. L: lumen (LM.
690 Mag: 20 x. Bar: 5 µm). **B.** Ultrastructure of the columnar epithelium of TM, showing
691 roundish-to-amoeboid shaped nuclei (N) delimited by a continuous nuclear membrane (nm).
692 Heterochromatin (He) was clustered in clumps or located as marginal patches under the
693 nuclear envelope among the dispersed euchromatin (Eu). The cytoplasm contains numerous
694 round or elongated mitochondria (m), with electron-dense lamellar cristae or electron-pale
695 content; lipid droplets (ld), short and long microvilli (mv), a few electron-negative vacuoles
696 (V) and secretory granules with a slightly electron-dense content (asterisks). The junctional
697 complexes between neighboring epithelial cells appear well-formed and constituted from the
698 lumen by *zonulae occludens* (arrow) followed by *zonulae adherens* (arrowhead) (TEM. Bar:
699 2 µm). **C.** CECs of TM showing a large multivesicular body (mvb), an electron-dense
700 secondary lysosome (Ly), tubular elements of the endoplasmic reticulum (ER), well-defined
701 nuclei (N) and mitochondria (m). V: vacuoles; mv: microvilli; Gl: glycogen granules;
702 asterisk: secretory granules (TEM. Bar: 1 µm). **D.** The luminal side (L) of TM shows
703 numerous short or long microvilli (mv). m: mitochondria; arrows: *zonulae occludens*;
704 arrowhead: *zonula adherens* (TEM. Bar: 1 µm). **E.** High magnification of motile cilia (Ci)
705 showing an evident axoneme of nine peripheral doublet microtubules, surrounding a central

706 complex with two central microtubules and the central sheath (9 + 2 arrangement). Gl:
707 glycogen granule; arrows: *zonula occludens* (TEM. Bar: 2 µm).

708

709 **Figure 2. 4R group. A.** Representative picture of a transversal section of mouse ampulla
710 presenting a highly folded and branched *tunica mucosa* (TM), characterized by columnar
711 epithelial cells (CEC) with intensely stained prominent nuclei (asterisk). The outer and inner
712 layers of *tunica muscularis* (TMu) consist of longitudinal and circular fibers, respectively,
713 from the outer to the inner portion, similarly to the control group. L: lumen (LM. Mag: 20 x.
714 Bar: 5 µm). **B.** The surface of *tunica mucosa* shows round-to-ovoidal or irregularly shaped
715 nuclei (N) delimited by an uninterrupted electron-dense nuclear membrane (nm); the
716 chromatin was organized as in control group. The cytoplasmic membrane is folded in a
717 continuous layer of microvilli (mv). The cytoplasm contains multivesicular bodies (mvb),
718 well-defined junctional complexes (JC) and rare round/elongated electron-dense
719 mitochondria (m). Numerous damaged mitochondria with signs of swelling (sm) or
720 vacuolization (vm) are shown. He: heterochromatin; Eu: euchromatin (TEM. Bar: 2 µm). **C.**
721 Magnified micrograph of CECs with two evident nuclei containing patches of
722 heterochromatin (He) clustered under the nuclear membrane (nm). the microvillar coverage
723 (mv) shows numerous interruptions. Eu: euchromatin; nm: nuclear membrane; m:
724 mitochondria; sm: swollen mitochondria; vm: mitophagic vacuoles (TEM. Bar: 1 µm). **D.** a
725 detail of cytoplasm of an epithelial cell containing strongly indented nuclei, two
726 multivesicular bodies (mvb), an electron-dense granule (g) and lipid droplets (ld). Numerous
727 swelled mitochondria (sm) and mitophagic vacuoles (vm) are visible N: nucleus (TEM. Bar:
728 1 µm). **E.** High magnification of a nucleus (N) with a nucleolus (Nu) surrounded by

729 vacuolated mitochondria (vm) with marginalized content (TEM. Bar: 1 μ m). *Inset*. Swollen
730 mitochondria (sm) with evident signs of matrix and cristae degeneration (TEM. Bar: 0,6 μ m).
731 **F.** Detail of a big intracytoplasmic vacuole (*) lined by microvilli. N: nucleus; m:
732 mitochondria; sm: swollen mitochondria; vm: mitophagic vacuole (TEM. Bar: 1 μ m).

733

734 **Figure 3. 8R group. A.** Representative image of a semithin section of the ampullar region
735 of mouse FTs showing the highly folded *tunica mucosa* (TM) with big nuclei (asterisk) and
736 the well-defined two layers of *tunica muscularis* (TMu) and the *tunica serosa* (TS). CECs:
737 columnar epithelial cells, L: lumen (LM. Mag: 20 x. Bar: 5 μ m). **B.** Micrograph of the *tunica*
738 *mucosa* showing nuclei (N), round/elongated electron-dense mitochondria (m), endoplasmic
739 reticulum (ER) tubules/networks, secondary lysosomes (Ly), microvilli (mv) and junctional
740 complexes (JC). Eu: euchromatin; He: heterochromatin, sm: swollen mitochondria; vm:
741 vacuolated mitochondria (TEM. Bar: 1 μ m). **C.** Detail of damaged mitochondria showing
742 numerous mitophagic vacuoles (vm) characterized by partial or complete cristolysis and
743 peripheric accumulation of the mitochondrial remains. mv: microvilli; arrow: *zonula*
744 *occludens*; arrowhead: *zonulae adherens* (TEM. Bar: 0,8 μ m). **D.** Epithelial cells showing
745 interdigitated cell contacts (arrows). The cytoplasm contains irregularly shaped nuclei (N)
746 and numerous vacuolated mitochondria (vm). JC: junctional complexes (TEM. Bar: 1 μ m).
747 **E.** Cytoplasmic content of columnar epithelial cells showing numerous mitophagic vacuoles
748 (vm) in proximity to multivesicular bodies (mvp) and lysosomes (Ly). ld: lipid droplet; mv:
749 microvilli; m: mitochondria; N: nucleus (TEM. Bar: 1 μ m). **F.** High magnification of non-
750 ciliated cells rich in electron-dense secretory granules (Sg) with homogeneous content and
751 numerous long and thin microvilli (TEM. Bar: 1 μ m).

752

753 **Figure 4. Surface analysis by SEM.** A-B. Control group. **A.** Numerous tufts of cilia (Ci)
754 surrounded by short microvilli (mv) protrude into the lumen of the ampullar epithelium
755 (SEM. Bar: 30 μm). **B.** High magnification of a well-preserved tuft of cilia (Ci) (SEM. Bar:
756 3 μm). C-D. 4R group. **C.** Numerous, long and homogenously distributed microvilli (mv)
757 protrude from the globoid surface of epithelial cells (SEM. Bar: 3 μm). **D.** Detail of a
758 heterogeneous carpet of short microvilli (mv) (SEM. Bar: 2.5 μm).

759

760

761

762

763

764

765

766

767

768

769

770

771

772

773

774

Mitochondria	Normal			Damaged		
	CTR	4R	8R	CTR	4R	8R
Dimension (μm)	0.444 \pm 0.096	0.415 \pm 0.060	0.472 \pm 0.086	0.553 \pm 0.118 ^a	0.659 \pm 0.099 ^b	0.817 \pm 0.179 ^c
Numerical density (N)	40 \pm 12.1 ^a	5.3 \pm 0.5 ^b	9.6 \pm 4.1 ^b	22.3 \pm 2.3 ^a	57.6 \pm 7.3 ^b	33 \pm 7.8 ^a
Percentage (%)	63.335 \pm 7.629 ^a	8.550 \pm 1.410 ^b	21.897 \pm 4.405 ^c	36.665 \pm 7.629 ^a	91.450 \pm 1.410 ^b	78.103 \pm 4.405 ^c

775

776 **Table 1. Morphometric analysis.** Dimension (μm), numerical density (N) and percentage
777 (%) of normal and damaged mitochondria from columnar epithelial cells of mouse fallopian
778 tube from control (CTR) and after four (4R) and eight (8R) rounds of repeated COH. The
779 morphometric analysis was performed on a 100 μm^2 epithelial area in low-magnification
780 TEM micrographs, from at least three sections from three different experiments per group.
781 Approximately, 40 mitochondria were measured per each experimental group (9-11
782 mitochondria/animal for control group (N=4 animals); 6-8 mitochondria/animal for 4R (N=6
783 animals); 8-10 mitochondria/animal for 8R (N=5 animals). Values of each group were
784 expressed as mean \pm SD. The percentages of normal or damaged mitochondrial frequency
785 were calculated over the total numerical density. Different superscripts indicate significant
786 differences among the groups of normal or damaged mitochondria ($P < 0.05$).

787

Figure 1

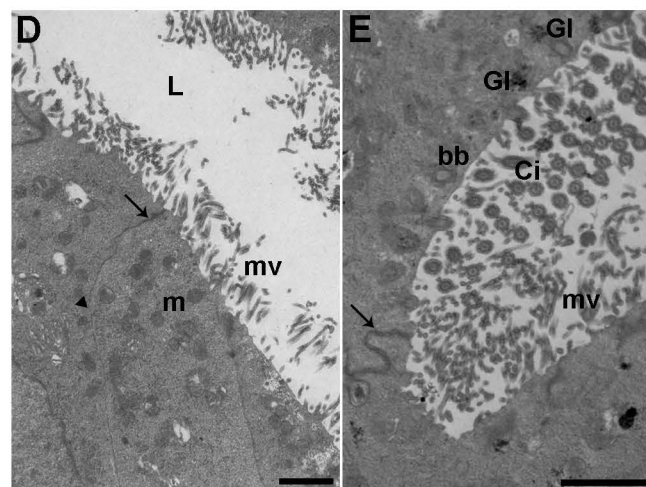
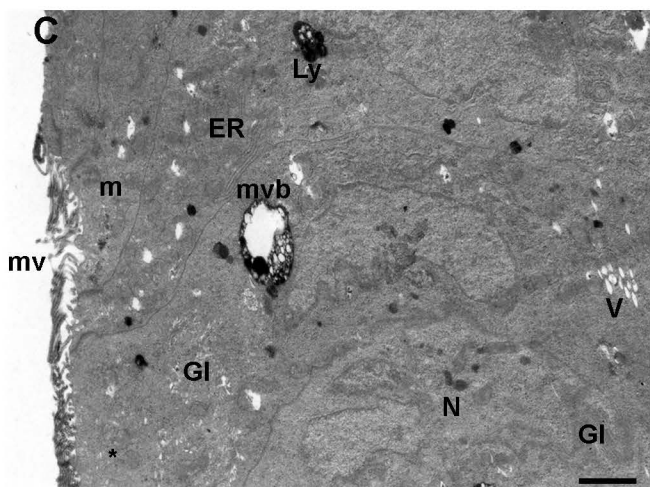
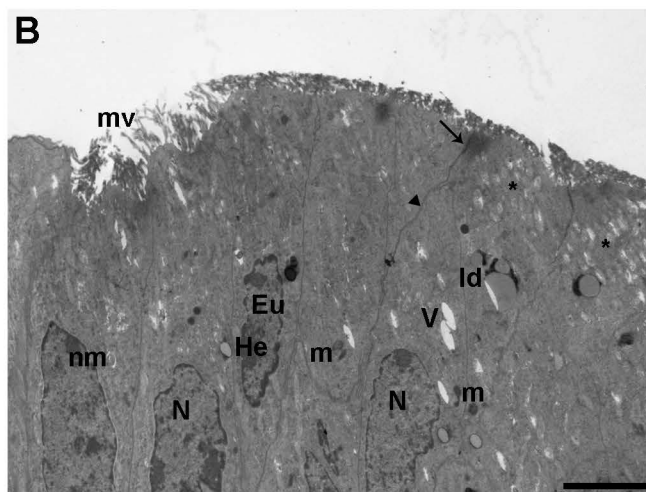
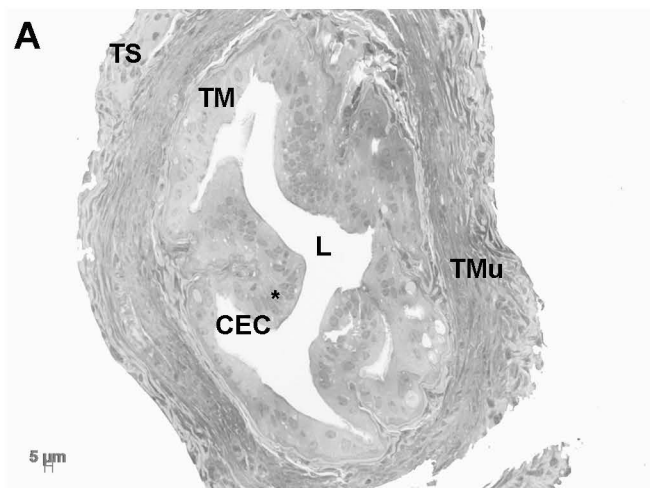


Figure 2

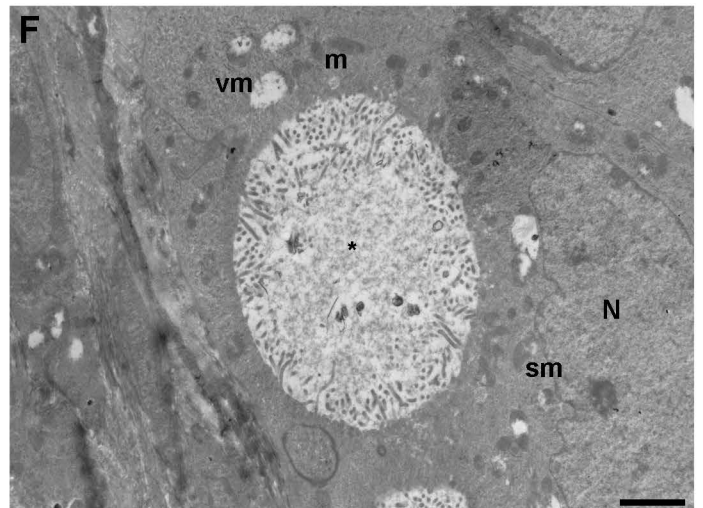
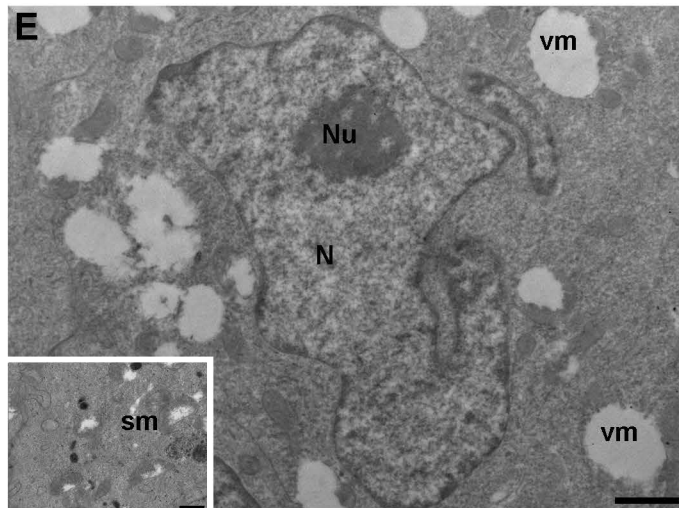
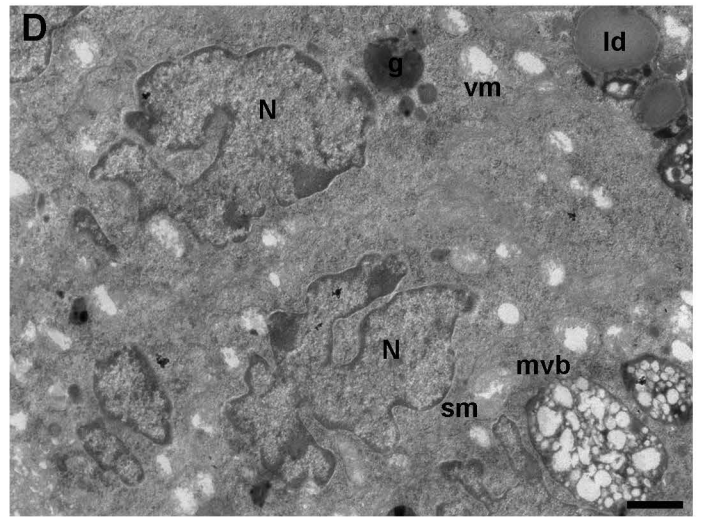
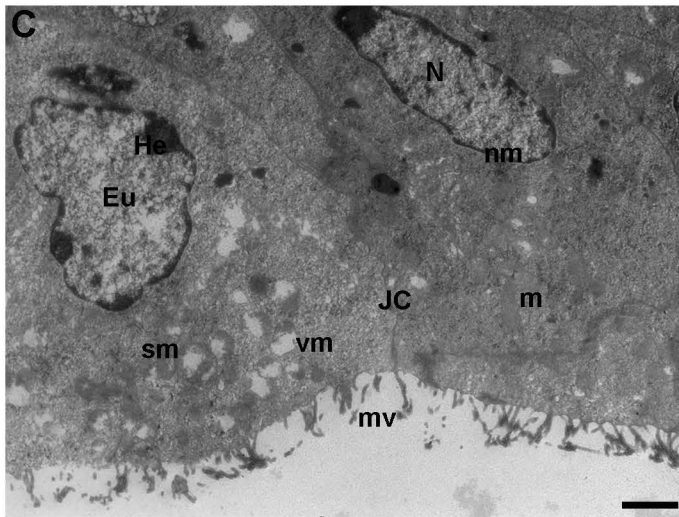
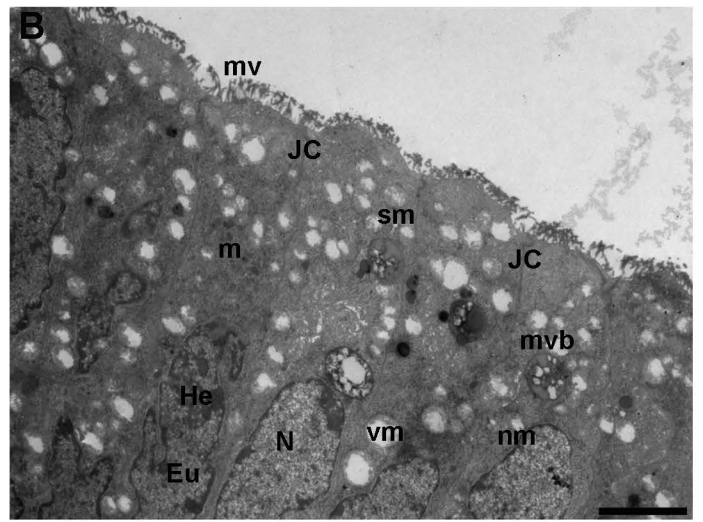
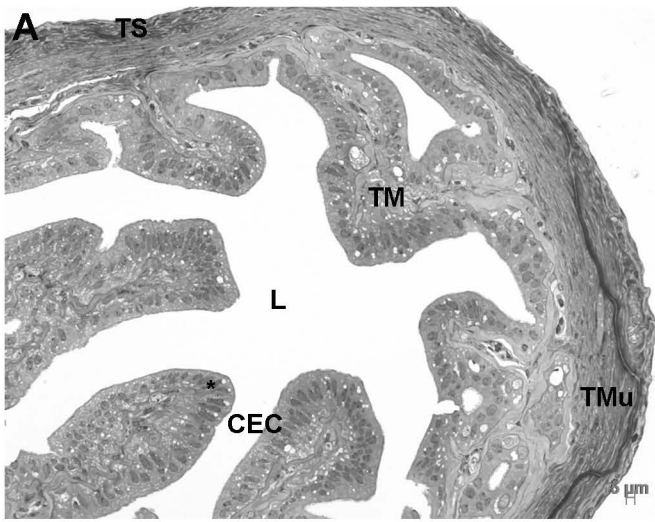


Figure 3

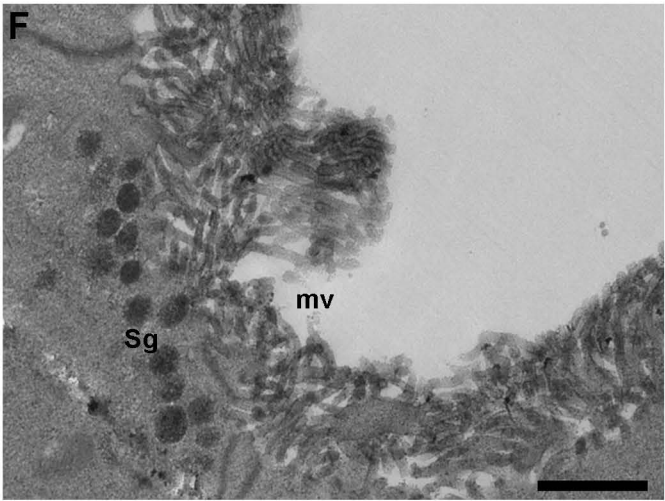
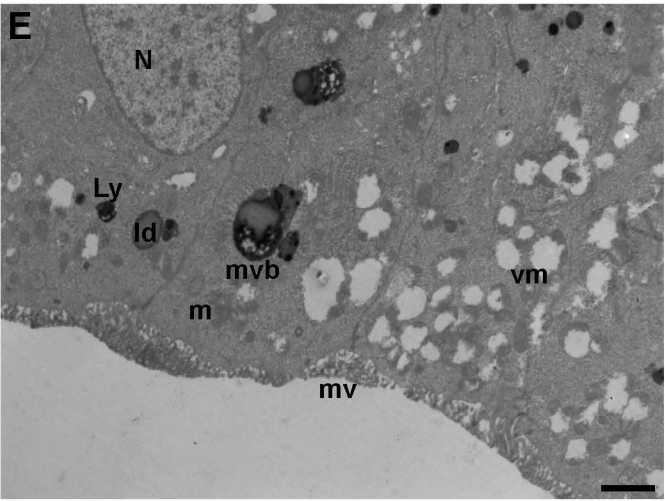
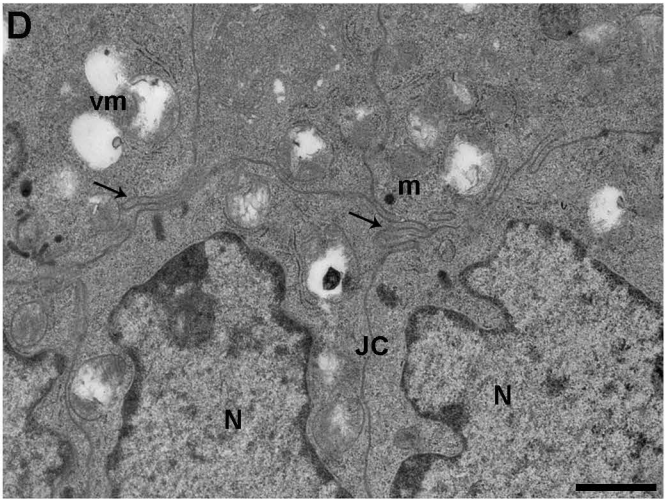
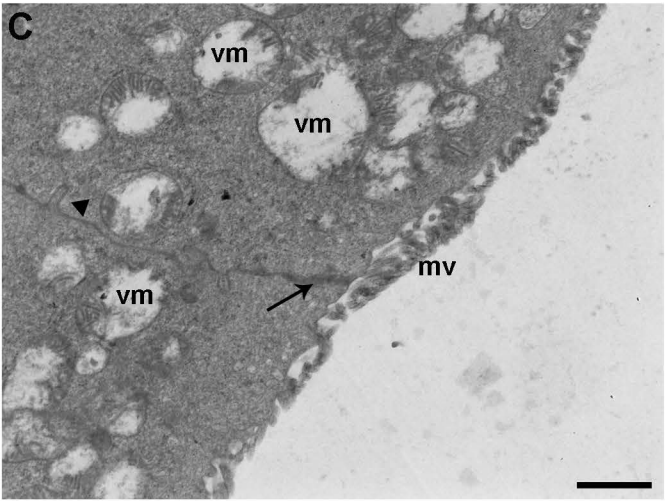
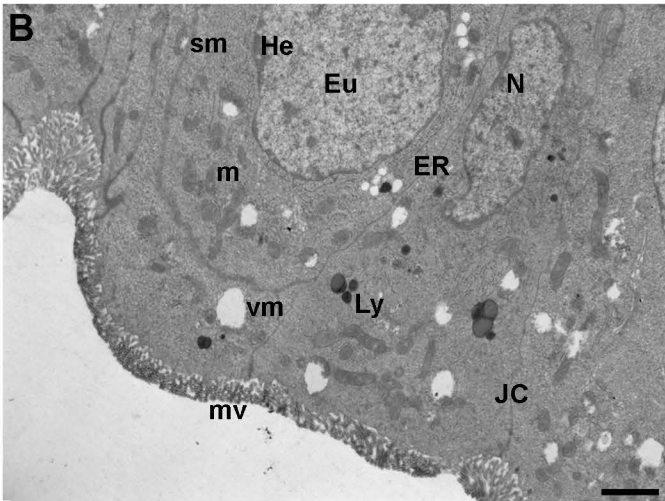
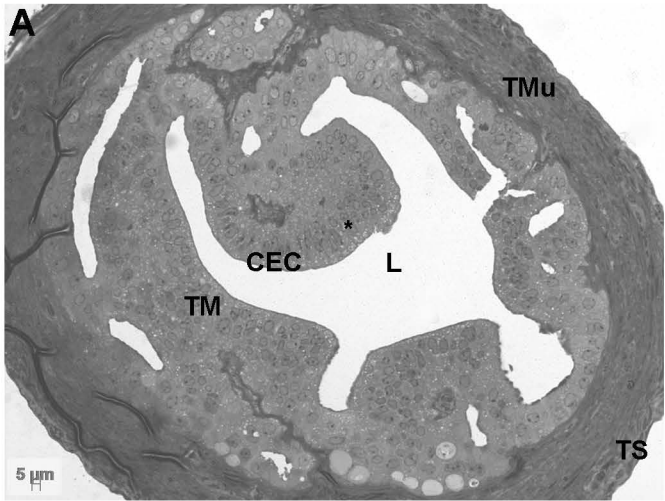


Figure 4

